Phase and group velocity tracing analysis of projected wave packet motion along oblique radar beams ? qualitative analysis of QP echoes

F. S. Kuo, H. Y. Lue, C. L. Fern

Ann. Geophys., 25, 77–86, 2007
www.ann-geophys.net/25/77/2007/

Annales Geophysicae

Phase and group velocity tracing analysis of projected wave packet motion along oblique radar beams – qualitative analysis of QP echoes

F. S. Kuo[1], **H. Y. Lue**[2], **and C. L. Fern**[3]

[1]Department of Electro-Optical Engineering, Van Nung University, Chung-Li, Taiwan
[2]Department of Physics, Fu-Jen Catholic University, Hsin-Chuang, Taiwan
[3]General Education Center, National Yunlin University of Science and Technology, Touliu, Yunlin, Taiwan

Received: 14 May 2006 – Revised: 11 December 2006 – Accepted: 20 December 2006 – Published: 1 February 2007

Abstract. The wave packets of atmospheric gravity waves were numerically generated, with a given characteristic wave period, horizontal wave length and projection mean wind along the horizontal wave vector. Their projection phase and group velocities along the oblique radar beam (v_{pr} and v_{gr}), with different zenith angle θ and azimuth angle ϕ, were analyzed by the method of phase- and group-velocity tracing. The results were consistent with the theoretical calculations derived by the dispersion relation, reconfirming the accuracy of the method of analysis. The RTI plot of the numerical wave packets were similar to the striation patterns of the QP echoes from the FAI irregularity region. We propose that the striation range rate of the QP echo is equal to the radial phase velocity v_{pr}, and the slope of the energy line across the neighboring striations is equal to the radial group velocity v_{gr} of the wave packet; the horizontal distance between two neighboring striations is equal to the characteristic wave period τ. Then, one can inversely calculate all the properties of the gravity wave responsible for the appearance of the QP echoes. We found that the possibility of some QP echoes being generated by the gravity waves originated from lower altitudes cannot be ruled out.

Keywords. Ionosphere (Ionospheric irregularities; General or miscellaneous)

1 Introduction

An outstanding feature of the E-region FAI radar echoes at the mid-latitude locations is a "quasi-periodic" (QP) type of echo, which appeared intermittently in time with periods of 5 to 10 min, about 100 km altitude during the post-sunset hours (Yamamoto et al., 1991; Ogawa et al., 1995). The QP echoes displayed wave-like features that resemble those of gravity waves in the atmosphere (Yamamoto et al., 1994), and they were proposed to be the result of the altitude modulation of Es layers by short-period gravity waves (Woodman et al., 1991; Tsunoda et al., 1994). It was pointed out (Fukao et al., 1998) that the range rate of QP echoes detected with the MU radar (pointing northward at zenith angle ∼50 degrees) was almost always negative (i.e. toward the radar), about −60 to −90 m/s. The direction of propagation of the QP echo regions is sharply peaked in the southwestward direction (Tanaka and Venkateswaren, 1982; Riggin et al., 1986; Yamamoto et al., 1994), and the FAI drift speed is usually larger than 100 m/s (Yamamoto et al., 1994). OH airglow (about 87 km altitude) observed with CCD imager (Nakamura et al., 1998) during the 1996 SEEK (SEEK-1) campaign period (Fukao et al., 1998) revealed that the distributions of the horizontal wavelength, observed wave period, and horizontal phase speed were found to be 10–30 km, 5–30 min, and 20–60 m/s, respectively, and the horizontal propagation direction was mainly northeastward. Such an inconsistency between the propagation directions of the horizontal phase velocities seemed to rule out the possibility that QP echoes were generated by the gravity waves that originated from lower altitudes.

Since the SEEK-1 campaign, many more experiments were conducted to explore the physics of QP echoes. Among them, SEEK-2 (Yamamoto et al., 2005) is the most intensive observation campaign to study the spatial structure of the field-aligned irregularity (FAI) and sporadic-E (Es) layer. This campaign, along with SEEK-1, confirmed that the QP echoes are associated with Es-layers mainly around 105 km. Accumulation of the E-region plasma into the layers is well explained by the shear of the neutral wind (Bernhardt et al., 2005; Larsen et al., 2005; Pfaff et al., 2005; Wakabayashi and Ono, 2005; Yokoyama et al., 2005). The Es-layers are spatially modulated by the motion of the neutral atmosphere (Maruyama et al., 2006), and then FAI echoes start to appear. The sources of the FAIs are the plasma-density gradient of

Correspondence to: F. S. Kuo
(fskuo@msa.vnu.edu.tw)

Published by Copernicus GmbH on behalf of the European Geosciences Union.

the Es-layers and the polarization electric field induced by the neutral wind and the spatial inhomogeneity of the Es-layers. The source of the QP echoes in the main Es-layers can be a gravity wave or Kelvin-Helmholtz (K-H) instability in the neutral atmosphere (Larsen, 2000). Another possible source is the azimuth-dependent E-region instability, which predicts a southwestward propagation of the QP echo region with phase front aligned from northwest to southeast (Cosgrove and Tsunoda, 2002, 2003). However, by simultaneous observations of the atmospheric gravity waves (AGWs) in OI and OH airglow images and the VHF radar backscatter from field-aligned irregularities (FAI) during the SEEK-2 campaign, Onoma et al. (2005) found that AGWs tended to propagate southeastward during FAI events. This result suggests that the interaction between AGW and E-region plasma plays an important role in generating FAI. Ogawa et al. (2005) compared the data of the QP echoes (as the height of QP echoes was low) and the air glow at the same altitude, and found a positive correlation between the height variation of FAI echoes and airglow intensity. Also, Saito et al. (2005) conducted simultaneous observations of FAIs and neutral wind with interferometry measurements, and found that QP echoes propagated northwestward when the rockets were launched. Hysell et al. (2004) reported results from simultaneous observations with Arecibo IS radar and a 30-MHz imaging radar. They used the imaging radar technique and found that the southwest-propagating structures elongated from northwest to southeast, which is a favorable alignment for the azimuth-dependent instability process. In their paper, they suggested the KH instability as the source of the QP structure but reached no clear conclusion. All these results indicate that there may be more than one mechanism responsible for the QP echo generation, and AGW is one of them to be investigated.

It should be helpful to study the properties of propagation of AGWs along the radar beam and compare them to those of QP echoes. None of the existing theories on QP echoes has ever taken the group velocity of gravity wave into consideration. It is well known that (Kuo et al., 2003; Kuo and Röttger, 2005) the vertical phase velocity of an atmospheric gravity wave may be in either the opposite or the same direction as its vertical group velocity, depending on the relation between its horizontal phase velocity v_{ph} and the projection mean wind velocity u_h. If $u_h < v_{ph}$, the phase and group velocities will have an opposite sense of vertical propagation (called Type 1 wave packet). Otherwise ($v_{ph} < u_h$), they will have the same sense of vertical propagation (called Type 2 wave packet). Here u_h is the projection wind velocity along the horizontal direction of phase propagation (so, $v_{ph} \geq 0$ always). Therefore, group velocity is a valuable parameter (in addition to wave period and phase velocity) to characterize the gravity wave. And a method called phase- and group-velocity tracing was developed (Kuo et al., 1998) to analyze the phase- and group-velocities of any kind of wave propagation.

The technique of velocity tracing was applied to analyze the data observed by SOUSY-Svalbard Radar in October 2000 in the altitude range between 2.4 km and 17.4 km (Kuo et al., 2003), in which hundreds of wave packets with characteristic wave periods in the range 15∼45 min were identified from Range-Time-Intensity (RTI) plots: About 85% of them were Type 1 wave packets, revealing the typical characteristics of the propagation of atmospheric gravity waves in the linear regime; About 15% were Type 2 wave packets. Then, for another set of data taken during the period between 30 March and 24 April in 2000, in the altitude range between 2.85 km and 14.85 km, also using the SOUSY Svalbard Radar, with the simultaneous information on the background wind also available, not only the horizontal wavenumber component of a wave packet along the direction of the background wind velocity was calculated by the dispersion equation, but also the angle between the horizontal wave vector and its background wind velocity was obtained by the polarization equation of gravity wave (Kuo and Röttger, 2005). Again, most of the wave packets (76%) with characteristic wave period of ∼70 min in the Range-Time-Intensity (RTI) plots of velocity were type 1 wave packets, and the rest (24%) were type 2 wave packets. In this study we will assume the striated structure of the QP echoes to be possibly the result of the projection movement of the gravity wave packet along the radial direction of the obliquely pointing radar beam. This assumption is intuitively based on the similarity between the striation structure of QP echoes and the RTI plot of the gravity wave packet motion obtained by numerical simulation. The physics behind this assumption will be discussed in Sect. 2. Based on the information on the projection phase and group velocities along the obliquely pointing radar beam, we shall be able to recover the horizontal and vertical propagation of the gravity wave packet. Such a process of analysis should be able to reduce the uncertainty in studying the generation mechanism of QP echoes.

2 Conjecture on QP echoes

The similarity between the striated structure of the QP echoes and the RTI plot of the gravity wave packet motion obtained by numerical simulation prompted us to assume that the QP echoes is possibly the result of the projection motion of the gravity wave packet along the radar beam. It is known that QP echoes originate from the structured Es layer at altitudes around 100 km (Ogawa et al., 2002). The polarization electric field induced by the neutral wind or external electric field is mapped along the geomagnetic field line, and induces plasma irregularities striated along the geomagnetic field line (Maruyama et al., 2000; Yokoyama et al., 2003, 2004). The radar returns from the QP echo region are most likely the result of gradient drift instability associated with the Es layer.

The linear theory of electro-jet instability (Fejer et al., 1975) yielded the following expression for both the gradient

drift and two-stream modes:

$$\omega_r = \boldsymbol{k} \cdot (\boldsymbol{V}_e + \Psi \boldsymbol{V}_i) \big/ (1+\Psi) \tag{1a}$$

$$\gamma = \frac{\Psi}{(1+\Psi)\,\nu_i} \left\{ \left[\frac{\boldsymbol{k} \cdot (\boldsymbol{V}_e - \boldsymbol{V}_i)}{1+\Psi} \right]^2 - k^2 C_s^2 \right\} + \frac{\boldsymbol{k} \cdot (\boldsymbol{V}_e - \boldsymbol{V}_i)}{(1+\Psi)^2} \cdot \frac{1}{Lk^2} \cdot \frac{\nu_i k_\perp}{\Omega_i} - 2\alpha n_0 \tag{1b}$$

with

$$\Psi_0 = \frac{\nu_e \nu_i}{\Omega_e \Omega_i} \tag{1c}$$

$$\Psi = \Psi_0 \left[\left(k_\perp^2 \big/ k^2 \right) + \left(\Omega_e^2 \big/ \nu_e^2 \right) \left(k_{11}^2 \big/ k^2 \right) \right] \tag{1d}$$

under the assumption that the growth rate is much smaller than the wave frequency, i.e. $\gamma \ll \omega_r$. In these equations, L is the vertical plasma density gradient scale length, α is the recombination rate, ω_r is the frequency and $\boldsymbol{k}$ is the wave vector of the gradient drift wave (or two-stream wave), k_{11} ($k_\perp$) is the wave vector component parallel (perpendicular) to the magnetic field, $\boldsymbol{V}_e (= \boldsymbol{E}_0 \times \boldsymbol{B}_0 \big/ B_0^2)$ is the drift velocity of electrons and $\boldsymbol{V}_i$ is the zero order velocity of ions, ν_e, ν_i, Ω_e and Ω_i are the electron-neutral collision frequency, ion-neutral collision frequency, electron-gyrofrequency and ion-gyrofrequency, respectively.

As the irregularities associated with QP echoes are most likely generated by the gradient drift instability of the Es layer, we shall consider only the second and third terms in Eq. (1b) by setting $\Psi = \Psi_0$ (because for FAI, $k \cong k_\perp$)

$$\gamma_{GD} = \frac{\boldsymbol{k} \cdot (\boldsymbol{V}_e - \boldsymbol{V}_i)}{(1+\Psi_0)^2} \cdot \frac{\nu_i}{\Omega_i L k} - \frac{\Psi_0 k^2 C_s^2}{(1+\Psi_0)\,\nu_i} \,. \tag{2}$$

Since $\Omega_i \ll \nu_i$ in the region of interest, the zero-order velocity of ions $\boldsymbol{V}_i$ would be approximately equal to the neutral wind velocity $\boldsymbol{U}_n$, i.e. $\boldsymbol{V}_i \approx \boldsymbol{U}_n$ in Eq. (2). Since the time (spatial) scale of atmospheric gravity waves is much larger than that of gradient drift waves, we may regard the instant neutral wind velocity $\boldsymbol{U}_n = \boldsymbol{U}_0 + \delta \boldsymbol{u}_n$ as the background mean wind velocity encountered by the gradient drift waves, where $\boldsymbol{U}_0$ is the mean wind velocity encountered by the gravity waves, and $\delta \boldsymbol{u}_n$ is the fluctuation velocity contributed by the gravity waves. So the growth rate γ_{GD} will be modulated by the gravity wave motion through the factor $G = \boldsymbol{k} \cdot (\boldsymbol{V}_e - \boldsymbol{U}_0 - \delta \boldsymbol{u}_n)$. To be more explicit, let the first term of the right-hand side of Eq. (2) be expressed as $A \cdot G$. In the case with $A > 0$, γ_{GD} will be maximum (minimum) and will result in maximum (minimum) radar echo power, if $\boldsymbol{k} \cdot \delta \boldsymbol{u}_n$ is minimum (maximum). When $A < 0$, the situation is reversed. This explains why the striated structure of the QP echoes might be the result of the projection motion of the wave packet of the atmospheric gravity waves along the radar beam. Since the echo power is directly related to $\delta \boldsymbol{u}_n$, and not to the square of $\delta \boldsymbol{u}_n$, the horizontal distance between two consecutive striations should be equal to the characteristic wave period of the QP echoes (not half period). We also notice that there will be no gravity wave modulation on the gradient drift instability, if $\boldsymbol{k} \cdot \delta \boldsymbol{u}_n = 0$.

Due to the energy conservation principle, the amplitude of $\delta \boldsymbol{u}_n$ is inversely proportional to the square root of the density of the atmosphere. To obtain some idea about the magnitude of $\delta \boldsymbol{u}_n$ in the QP echo region, let's roughly assume the scale height of the atmosphere to be $\approx$8 km. Then the amplitude of $\delta \boldsymbol{u}_n$ will increase by a factor of 23 (277) as the gravity wave propagates upward from the altitude of 50 km (10 km) to the altitudes of QP echoes around 100 km. Therefore, the amplitude of the AGW in the QP echo region will be very likely large enough to modulate the FAI. A clear evidence of gravity wave modulation was presented by Ogawa et al. (2005). They reported that during the QP echo event, the echo altitudes clearly went up (down) in harmony with an airglow enhancement (subsidence). The air glow intensity, QP radar echo intensity, and Doppler velocity of FAIs at around 96-km altitude fluctuated with periods from 10 min to 1 h, indicating that these parameters were modulated with short-period atmospheric disturbances. Some QP echo regions below 100-km altitude contained small-scale QP structures in which a very strong neutral wind exceeding 100 m/s existed.

Woodman et al. (1991) pointed out that in the mid-latitude region where the magnetic dip angle is large, ionospheric conditions at other altitudes on the same magnetic field line must be taken into account. Because of the high conductivity along the inclined magnetic field lines, the electric field induced by $\delta \boldsymbol{u}_n$ associated with AGWs, might be cancelled before acting on the electron density gradient, if the wave front of AGW is not parallel to the magnetic field line. So we shall further assume that QP echoes might be the result of the specific atmospheric gravity waves propagating with their wave fronts parallel to the magnetic field lines.

3 Wave packet motion observed by oblique radar beam

3.1 Theory

Assume that the gravity wave propagating in the atmosphere follows the dispersion relation, neglecting vertical wind shear,

$$k_z^2 = \left(\frac{\omega_b^2}{\omega^2} - 1 \right) k_h^2 - \frac{1}{4H^2} \tag{3}$$

$$\omega = \sigma - k_h \cdot u_h \,, \tag{4}$$

where ω_b, ω, σ, k_h and k_z are the Brunt-Väisälä frequency, intrinsic frequency, observed frequency, horizontal wave number and vertical wave number, respectively; H is the scale height of the atmosphere, and u_h is the projection wind velocity along the horizontal wave number vector $\boldsymbol{k}_h$. Substituting Eq. (4) into (3) yields the observed frequency σ as

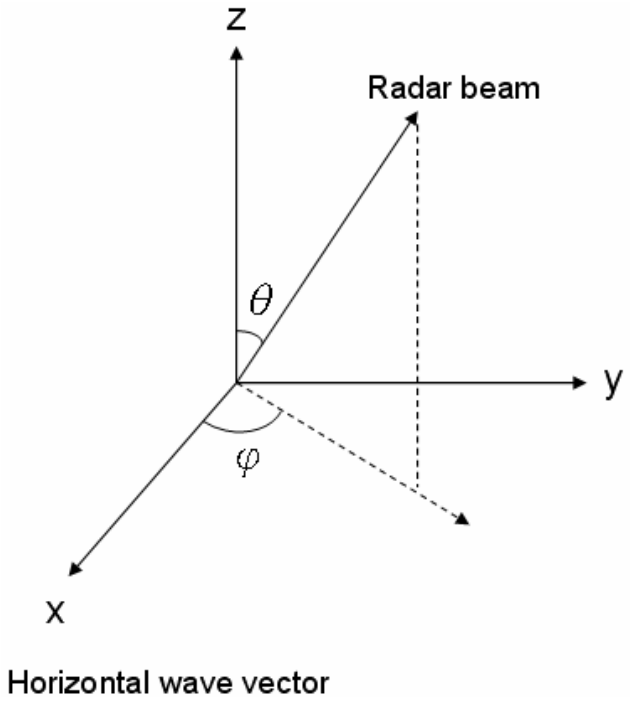

Fig. 1. Relative directions of the radar beam and the horizontal wave vector of gravity wave.

a function of k_h and k_z. The horizontal and vertical phase velocities v_{ph} and v_{pz} are readily defined by

$$v_{ph} = \sigma / k_h \tag{5}$$

$$v_{pz} = \sigma / k_z \quad . \tag{6}$$

The horizontal and vertical group velocities v_{gh} and v_{gz} of the wave propagation are

$$v_{gh} = \left(\frac{\partial \sigma}{\partial k_h}\right)_{k_z} = u_h + \left(v_{ph} - u_h\right) \cdot \left(1 - \frac{\omega^2}{\omega_b^2}\right) \tag{7}$$

$$v_{gz} = \left(\frac{\partial \sigma}{\partial k_z}\right)_{k_h} = -\left(v_{ph} - u_h\right)^2 \cdot \left(\frac{\omega}{\omega_b}\right)^2 \left(\frac{k_z}{\omega}\right). \tag{8}$$

In the case with the radar beam pointing obliquely with zenith angle θ, it is more convenient to describe the wave propagation in the spherical coordinate system, as shown in Fig. 1. Let's define the horizontal wave number vector in the positive x-direction, i.e. $\boldsymbol{k}_h = k_h \boldsymbol{a}_x$. Then the wave number vector of gravity wave can be expressed in both the Cartesian system and the spherical system as follows,

$$\boldsymbol{k} = k_h \boldsymbol{a}_x + k_z \boldsymbol{a}_z = k_r \boldsymbol{a}_r + k_\theta \boldsymbol{a}_\theta + k_\phi \boldsymbol{a}_\phi,$$

where k_r is the wave number component along the radar beam, θ is the zenith angle of the oblique radar beam, and ϕ is the angle between the two vertical planes: one containing the radar beam and the other one containing the wave vector $\boldsymbol{k}$. The transformations of the wave number components between the two coordinate systems are given by

$$k_x = k_h = k_r \cdot \sin\theta \cdot \cos\phi + k_\theta \cdot \cos\theta \cdot \cos\phi - k_\phi \cdot \sin\phi \tag{9a}$$

$$k_y = 0 = k_r \cdot \sin\theta \cdot \sin\phi + k_\theta \cdot \cos\theta \cdot \sin\phi + k_\phi \cdot \cos\phi \tag{9b}$$

$$k_z = k_r \cdot \cos\theta - k_\theta \cdot \sin\theta, \tag{9c}$$

and inversely,

$$k_r = k_h \cdot \sin\theta \cdot \cos\phi + k_z \cdot \cos\theta \tag{10a}$$

$$k_\theta = k_h \cdot \cos\theta \cdot \cos\phi - k_z \cdot \sin\theta \tag{10b}$$

$$k_\phi = -k_h \cdot \sin\phi \quad . \tag{10c}$$

Since the phase velocities are inversely proportional to the wave numbers, i.e. $v_{ph} = \sigma / k_h$, $v_{pz} = \sigma / k_z$, $v_{pr} = \sigma / k_r$, $v_{p\theta} = \sigma / k_\theta$, and $v_{p\phi} = \sigma / k_\phi$, the transformations among the phase velocity components can be obtained from Eqs. (10a, b, c),

$$v_{pr}^{-1} = v_{ph}^{-1} \cdot \sin\theta \cdot \cos\phi + v_{pz}^{-1} \cdot \cos\theta \tag{11a}$$

$$v_{p\theta}^{-1} = v_{ph}^{-1} \cdot \cos\theta \cdot \cos\phi - v_{pz}^{-1} \cdot \sin\theta \tag{11b}$$

$$v_{p\phi}^{-1} = -v_{ph}^{-1} \cdot \sin\phi \quad . \tag{11c}$$

Notice that the frequency is invariant under coordinate transformation, i.e. $\sigma(k_h, k_z) = \tilde{\sigma}\left(k_r, k_\theta, k_\phi\right)$, and $\omega(k_h, k_z) = \tilde{\omega}\left(k_r, k_\theta, k_\phi\right)$. Then the projection group velocity along the radar beam v_{gr} is given by

$$v_{gr} = \left(\frac{\partial \tilde{\sigma}}{\partial k_r}\right)_{k_\theta, k_\phi} = \left(\frac{\partial \tilde{\omega}}{\partial k_r}\right)_{k_\theta, k_\phi} + u_h \cdot \left(\frac{\partial k_h}{\partial k_r}\right)_{k_\theta, k_\phi} \tag{12a}$$

where

$$\left(\frac{\partial \tilde{\omega}}{\partial k_r}\right)_{k_\theta, k_\phi} = -\frac{\tilde{\omega}^3}{\omega_b^2 k_h^2}\left[k_r\left(\sin^2\theta \cdot \cos^2\phi + \cos^2\theta\right) + k_\theta \cos\theta \cdot \sin\theta \cdot \left(\cos^2\phi - 1\right) - k_\phi \sin\theta \cdot \cos\phi \cdot \sin\phi\right] + \frac{\tilde{\omega}}{k_h}\sin\theta \cdot \cos\phi, \tag{12b}$$

$$\left(\frac{\partial k_h}{\partial k_r}\right)_{k_\theta, k_\phi} = \sin\theta \cdot \cos\phi \quad . \tag{12c}$$

The radial phase- and group-velocities v_{pr} and v_{gr} along the radar beam, as well as the frequency σ are indirectly observable by the oblique radar beam, which is required to probe the E-region ionospheric irregularities. The multi-beam observations by MU radar made it possible to measure the horizontal propagation velocity of the FAI irregularity region. So Eqs. (3–12) provide us with a tool to investigate the characteristics of the gravity wave propagation and the possibility of wave coupling into the E-region ionosphere from lower altitudes. There are two solutions of Eq. (3) for k_z: one positive and one negative, with equal amplitude, and only the wave with an upward group velocity can propagate into the FAI irregularity region from lower altitudes.

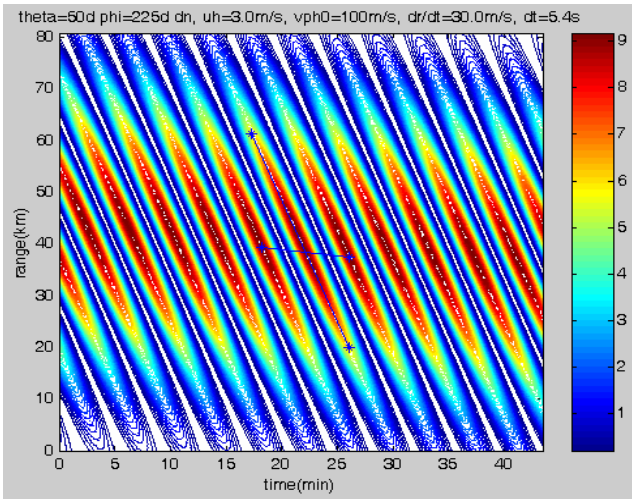

Fig. 2. RTI plot of the numerical gravity wave packet generated by Eq. (13) with following preset parameters: τ_0=7.5 min, v_{ph0}=100 m/s, τ_b=5.0 min, u_h=3 m/s, H=8 km, θ=50°, and ϕ=225°. The slope of the phase line along the central patch is equal to the characteristic radial phase velocity v_{pr}; the slope of the energy line across the neighboring patches is equal to the radial group velocity v_{gr}; the horizontal distance between two neighboring patches is equal to one-half of the wave period τ. The result of the measurements: τ=7.45 min, v_{pr}=−78.5 m/s, v_{gr}=−4.01 m/s. The theoretical prediction: τ=7.5 min, v_{pr}=−80.4 m/s, v_{gr}=−3.74 m/s.

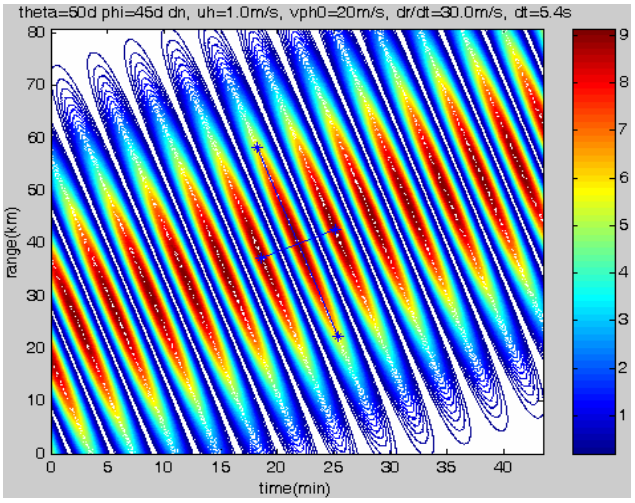

Fig. 3. Same as Fig. 2, except that the preset parameters were: τ_0=7.5 min, v_{ph0}=20 m/s, τ_b=5.0 min, u_h=1.0 m/s, H=8 km, θ=50°, and ϕ=45°. The result of the measurements: τ=7.64 min, v_{pr}=−83.8 m/s, v_{gr}=+13.8 m/s. And the theoretical prediction: τ=7.5 min, v_{pr}=−82.8 m/s, v_{gr}=+12.7 m/s.

3.2 Simulation of radial projection propagation of gravity wave packets

The properties (k_z, k_r, k_θ, k_ϕ) of a gravity wave specified by its wave frequency σ and horizontal wave number k_h are determined by the dispersion relations (3) and (4) and the transformations (10a, b, c). An oblique radar beam (almost perpendicular to the magnetic field line to probe FAI), pointing to the direction defined by the angles ϕ and θ, will detect the frequency σ and radial wave number k_r. Since the atmospheric gravity wave is a highly localized phenomenon, the radar beam will see a group of waves (which form a wave packet) rather than a single wave. A wave packet characterized by its central horizontal wave number k_{h0} and frequency σ_0 can be represented by the following equation

$$\Theta(r,t) = \sum_{\sigma} \exp\left[-(\sigma-\sigma_0)^2 \Big/ \sigma_s^2\right] \cdot \cos\left[\sigma(t-t_0) - k_r(r-r_0)\right], \quad (13)$$

where $\Theta(r,t)$ is an observable quantity to be detected by the radar beam, and σ_s represents the spectral width of the wave packet. The observed frequency σ and radial wave number k_r must satisfy the governing Eqs. (3, 4) and (9, 10). An example of the RTI plot of the numerical wave packet generated by Eq. (13) and converted by the phase and group velocity tracing technique (Kuo et al., 1998) is demonstrated in Fig. 2. A brief description of the velocity tracing technique is presented in Appendix A. The given parameters of the numerical wave packet in Fig. 2 were $\tau_0=1/\sigma_0$=7.5 min, $v_{ph0}=v_{px0}$=100 m/s; the atmospheric parameters were $\tau_b=1/\omega_b$=5.0 min, u_h=3.0 m/s, H=8.0 km; the radar beam direction was given by θ=50° and ϕ=225°. These parameters correspond approximately to a situation of the MU radar experiment in which a southwestward propagating gravity wave was encountered by the radar beam pointing northward with the zenith angle of θ=50°. According to the method of phase- and group-velocity tracing, the slope of the phase line along each striation is equal to the characteristic radial phase velocity v_{pr}; the slope of the energy line across the neighboring striations is equal to the effective radial group velocity v_{gr}; the horizontal distance between two neighboring striations is equal to one-half of the characteristic wave period τ. The result of the measurement of the wave packet in Fig. 2 was: τ=7.45 min, v_{pr}=−78.5 m/s, v_{gr}=−4.01 m/s. This measured wave period (7.45 min) is close to the preset wave period (7.5 min) within 0.67%. Also, Eq. (11a) yields the projection radial phase velocity v_{pr}=−80.4 m/s, and Eq. (12a) yields the radial group velocity v_{gr}=−3.74 m/s. The difference between the results of the simulation and theory were 2.36% for radial phase velocity and 7.22% for radial group velocity. Another example of the RTI plot of wave packet motion generated by Eq. (13) is demonstrated in Fig. 3, using another set of parameters: τ_0=7.5 min, v_{ph0}=20 m/s, τ_b=5.0 min, u_h=1.0 m/s, H=8.0 km, θ=50°, and ϕ=45°. These parameters correspond approximately to the northeastward propagating gravity wave detected by

Table 1. Charateristic propagation velocities of gravity waves calculated from the dispersion relation with τ_b=5.0 min, H=8.0 km, v_{ph}=100 m/s and downward vertical phase propagation. The radar beam direction is defined by θ=50° and ϕ=225°. All the velocities are in m/s, wave periods in min. The case in the 7th row corresponds to the numerical wave packet of Fig. 1.

τ (min)	u_h	v_{ph}	v_{pz}	v_{pr}	v_{gh}	v_{gz}	v_{gr}	v_{pr}/v_{gr}
5.5	+21	100	−109.7	−88.7	+59.3	+37.2	−8.22	+10.8
5.5	+26	100	−95.3	−82.2	+66.5	+35.2	−13.4	+6.13
5.5	+31	100	−83.5	−76.3	+72.9	+32.5	−18.6	+4.10
7.5	−6	100	−111.7	−89.5	+47.1	+47.4	+4.98	−18.0
7.5	−3	100	−104.2	−86.3	+51.4	+46.6	+2.09	−41.3
7.5	0	100	−97.6	−83.3	+55.6	+45.5	−0.82	+102
7.5	**+3**	**100**	**−91.6**	**−80.4**	**+59.4**	**+44.3**	**−3.74**	**+21.9**
7.5	+6	100	−86.2	−77.7	+63.1	+42.8	−6.64	+11.7
10	−30	100	−99.5	−84.2	+45.1	+55.2	+11.1	−7.59
10	−20	100	−83.9	−76.5	+56.8	+51.5	+2.34	−32.7
10	−10	100	−71.6	−69.5	+66.7	+46.5	−6.28	+11.1
10	0	100	−61.5	−63.0	+75.0	+40.7	−14.5	+4.34

the OH airglow (about 87 km altitude) observation with the CCD imager (Nakamura et al., 1998) during the SEEK-1 campaign. The result of the measurements in Fig. 3 were: τ=7.64 min, v_{pr}=−83.8 m/s, v_{gr}=+13.8 m/s; The theoretical values of v_{pr} and v_{gr} obtained from Eqs. (11a) and (12a) were −82.8 m/s and +12.7 m/s, respectively. Again, the simulation result is very close to the theoretical calculation. We studied in such a manner many numerical wave packets with different parameters (θ, ϕ, v_{px0}, τ_0, u_h), and the results of the analyses were all satisfactorily consistent with the theoretical calculations. We concluded from these simulation studies that, if QP echoes were the result of the projection movement of gravity wave packets along the radar beam, then we can identify the slope of each striation of QP echoes as the radial phase velocity v_{pr}; the slope of the straight line connecting the central points of the consecutive striations as the radial group velocity v_{gr}; the horizontal distance between two neighboring striations as the characteristic wave period (not half wave period, as explained in Sect. 2). Then the other properties of the gravity waves, v_{ph}, v_{gh}, v_{pz} and v_{gz}, may be theoretically calculated assuming u_h is known.

3.3 Theoretical calculation of radial projection movement of wave packets

As described in Sect. 3.1, given θ, ϕ, τ, v_{ph} and u_h, we are able to calculate all the rest of the gravity wave properties, including v_{gh}, v_{pz}, v_{gz}, v_{pr}, and v_{gr}. The striations of the QP echoes observed by the MU radar revealed a constant range rate over a large height range (more than 20 km), implying that the projection mean wind u_h (encountered by the gravity waves) was constant over this height range. Otherwise, the radial phase velocity would vary with height, and the striation should be curved. The constant projection mean wind u_h can be obtained by taking the time average and height average of the observational wind profile in the height range of QP echoes. One available wind profile was measured by Larsen et al. (1998) with the chemical release technique as part of the SEEK-1 campaign. It revealed that the wind had a southward component ∼40 m/s and a zonal component ∼0 m/s at the altitude of 100 km; a northward component ∼110 m/s and a westward component ∼30 m/s at the altitude of 110 km. The average direction of the neutral wind was mainly northwestward in the altitude range 95∼125 km (see Fig. 2 of Larsen et al., 1998). We projected this wind profile into a certain direction defined by ϕ, then took the height average of the projection wind profile over the altitude range 90∼125 km as the constant projection wind u_h. For the case of ϕ=225°, we obtained $u_h \cong -3.3$ m/s; when ϕ=45°, $u_h \cong +3.3$ m/s. All these constant projection wind u_h were characterized by small values. This estimation of projection wind is only qualitatively credible because the wind measurement (in 1996) and the observation of QP echoes (in 1989) were not carried out simultaneously.

Table 1 is the list of the propagation velocity components of gravity waves calculated from the dispersion relation characterized by θ=50°, ϕ=225°, τ_b=5.0 min, H=8.0 km, v_{ph}=100 m/s and v_{pz}<0 (downward vertical phase propagation). Also, the theoretical propagation velocities of gravity waves characterized by θ=50°, ϕ=45°, τ_b=5.0 min, H=8.0 km, v_{ph}=20∼60 m/s and v_{pz}<0 are presented in Table 2. Notice that the radial phase velocities v_{pr} in each case were purposely predetermined to be in the range between −60 m/s and −90 m/s, which is the range of the range rates of the striations of the QP echoes detected by MU radar. The projection mean wind u_h and the wave period were adjusted to yield the radial phase velocity in this range (−60∼−90 m/s). However, all the calculations to obtain these two tables were made without requiring the wave front to be parallel to the magnetic field line. Therefore, these

Table 2. Charateristic propagation velocities of gravity waves calculated from the dispersion relation with τ_b=5.0 min, H=8 km, v_{ph}=20∼60 m/s and downward vertical phase propagation. The radar beam direction is defined by θ=50° and ϕ=45°. All the velocities are in m/s, wave periods in min. The case in the 4th row corresponds to the numerical wave packet of Fig. 2.

τ(min)	u_h	v_{ph}	v_{pz}	v_{pr}	v_{gh}	v_{gz}	v_{gr}	v_{pr}/v_{gr}
5.5	+6	20	−16.5	−84.6	+14.3	+6.86	+12.2	−6.93
5.5	+7	20	−14.7	−59.7	+15.5	+6.19	+12.4	−4.81
5.5	+29	60	−32.1	−90.9	+53.2	+12.8	+37.0	−2.46
7.5	**+1**	**20**	**−16.4**	**−82.8**	**+12.4**	**+9.29**	**+12.7**	**−6.52**
7.5	+2	20	−15.0	−63.8	+13.5	+8.62	+12.9	−4.95
7.5	+18	60	−32.0	−90.3	+50.9	+17.2	+38.6	−2.34
10	−5.5	20	−16.6	−86.4	+9.64	+12.5	+13.2	−6.55
10	−4	20	−15.1	−64.1	+11.4	+11.5	+13.5	−4.75
15	−18	20	−16.6	−85.0	+4.76	+18.4	+14.4	−5.90
15	−16	20	−15.1	−65.0	+7.04	+17.1	+14.8	−4.39

Table 3. Charateristic propagation velocities of gravity waves calculated from the dispersion relation with τ_b=5.0 min, H=8 km, v_{ph}=60∼100 m/s and downward vertical phase propagation. The radar beam direction is defined by θ=50° and ϕ is either 202.5° or 213.75°. These waves have their wave fronts parallel to magnetic field line ($v_{pz}/v_{pN}=\tan\theta\cong$1.19). All the velocities are in m/s, and wave periods in minutes.

τ	u_h	v_{ph}	v_{pE}	v_{pN}	v_{pz}	v_{pr}	v_{gh}	v_{gz}	v_{gr}	v_{pr}/v_{gr}
ϕ=202.5°										
7	−5.5	80	−209	−86.6	−102.9	−66.3	30.2	38.7	3.54	−18.7
6.5	0	80	−209	−86.6	−103.8	−66.5	32.7	36.5	0.33	−201.5
6.5	0.5	80	−209	−86.6	−102.0	−66.0	33.5	36.4	−0.32	+206.3
6	6	80	−209	−86.6	−103.2	−66.3	36.0	34.1	−3.59	+18.5
5.5	12	80	−209	−86.6	−102.8	−66.2	39.4	31.6	−7.57	+8.75
ϕ=213.75°										
6.5	−2.5	80	−144	−96.2	−114	−73.5	28.1	36.4	5.54	−13.3
6	**3.5**	**80**	**−144**	**−96.2**	**−114**	**−73.5**	**31.4**	**34.1**	**1.9**	**−38.7**
5.5	**9.5**	**80**	**−144**	**−96.2**	**−114.4**	**−73.6**	**34.8**	**31.6**	**−1.79**	**+41.1**
5.3	12	80	−144	−96.2	−114.2	−73.6	36.3	30.6	−3.41	+21.6
6	2.5	70	−126	−84.2	−100.4	−64.5	26.4	30.4	2.7	−23.9
5.7	6	70	−126	−84.2	−99.2	−64.2	28.8	29.1	0.31	−207
5.5	8	70	−126	−84.2	−100	−64.4	29.8	28.1	−0.9	+71.6
5.3	10	70	−126	−84.2	−101	−64.7	30.8	27.2	−2.12	+30.5

waves might not be able to generate QP echoes due to high conductivity along the magnetic field lines.

To find the candidate atmospheric gravity waves which are able to generate QP echoes, we set a condition requiring their wave fronts to be parallel to the magnetic field line, namely $v_{pz}/v_{pN}=\tan\theta\cong$1.19, where v_{pN} represents the northward phase velocity component of the gravity wave. Table 3 is the list of propagation components of the gravity waves satisfying this condition. The waves in Table 3 are further characterized by: (1) having a westward phase velocity component exceeding 100 m/s, (2) having a radial phase velocities in the range −60∼−90 m/s, (3) having small wave periods close to the Brunt-Väisälä period τ_b. These features are consistent with that of the QP echoes detected by the MU radar (Yamamoto et al., 1991). It worth mentioning that the results of the theoretical calculation for the southeast-southward waves (with ϕ=157.5°, 146.25°) will be identical to that of the corresponding southwest-southward waves (with ϕ=202.5°, 213.75°), except for the sign of the eastward phase velocity component v_{pE}, because $\cos(2\pi-\phi)=\cos\phi$ and $\sin(2\pi-\phi)=-\sin\phi$.

One convenient parameter for a quick identification of the gravity wave is the velocity ratio v_{pr}/v_{gr}, as listed in the last column of these tables. The values of v_{pr}/v_{gr} revealed by

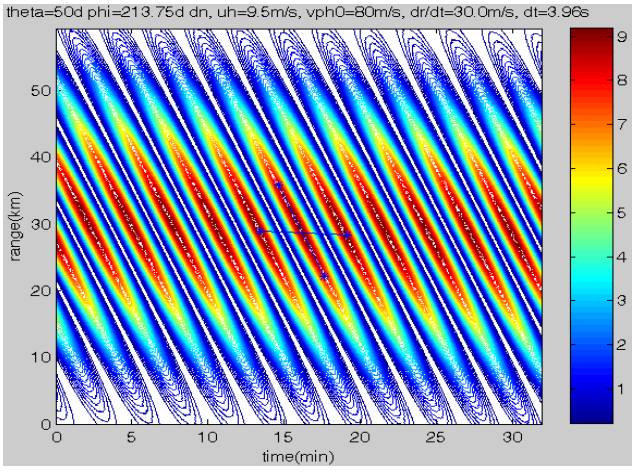

Fig. 4. Same as Fig. 2, except that the preset parameters were: τ_0=5.5 min, v_{ph0}=80 m/s, τ_b=5.0 min, u_h=9.5 m/s, H=8 km, θ=50°, and ϕ=213.75°. The result of the measurements: τ=5.59 min, v_{pr}=−76.1 m/s, v_{gr}=−1.68 m/s. And the theoretical prediction: τ=5.5 min, v_{pr}=−73.6 m/s, v_{gr}=−1.79 m/s.

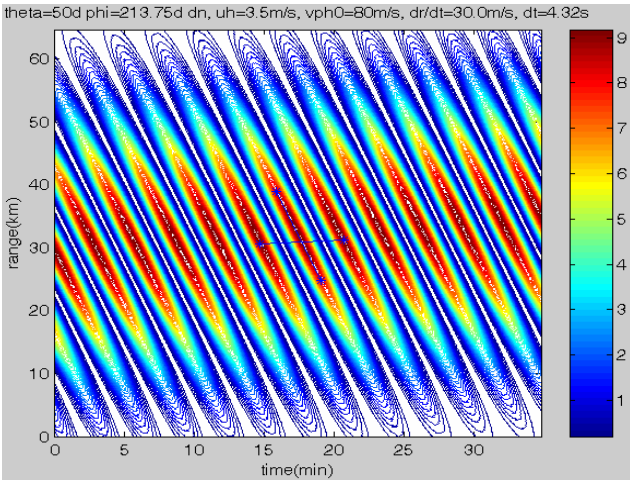

Fig. 5. Same as Fig. 2, except that the preset parameters were: τ_0=6.0 min, v_{ph0}=80 m/s, τ_b=5.0 min, u_h=3.5 m/s, H=8 km, θ=50°, and ϕ=213.75°. The result of the measurements: τ=6.15 min, v_{pr}=−73.8 m/s, v_{gr}=+1.75 m/s. And the theoretical prediction: τ=6.0 min, v_{pr}=−73.5 m/s, v_{gr}=+1.9 m/s.

QP echoes observed by Yamamoto et al. (1991) were characterized by a large positive value, in general. Experimentally, we can easily judge from Plate 1 and Plate 2 presented in the paper of Yamamoto et al. (1991) that both the slopes of the striations and the line across the striations were negative, in general, meaning that v_{pr}/v_{gr} was positive. There existed one exception: the radial group velocity in the time range 2230∼2250 and height range 92∼96 km was positive (see Plate 2 of Yamamoto et al., 1991), meaning that v_{pr}/v_{gr} was negative. Table 3 shows that the characteristic wave periods of the waves with negative v_{gr} (positive v_{pr}/v_{gr}) are smaller than those with positive v_{gr} (negativev_{pr}/v_{gr}). It seemed that smaller period waves were more effective than larger period waves in generating QP echoes detected by MU radar. The RTI plot of a candidate wave packet (with large positive v_{pr}/v_{gr}=+41.1) that is probably responsible for the generation of QP echoes is shown in Fig. 4. This wave packet is the same one presented in the 11th row of Table 3. The RTI plot of another candidate wave packet (with large negative v_{pr}/v_{gr}=−38.7) is shown in Fig. 5, with its parameters identical to that listed in the 10th row of Table 3. The measured values of τ, v_{pr}, and v_{gr} of these two candidate wave packets were found to be reasonably consistent with the theoretical calculations, as indicated in both figure captions.

From Tables 1–3, it can be readily found, as expected, that the values of the radial group velocities (v_{gr}) are related to the horizontal and vertical group velocities of (v_{gh} and v_{gz}) by the following equation,

$$v_{gr} = v_{gh} \cdot \sin\theta \cdot \cos\phi + v_{gz} \cdot \cos\theta. \quad (14)$$

Since this equation resembles the transformation of Eq. (10a), which is a coordinate transformation equation for the wave-vector components, we have confirmed that the group velocity of a wave packet indeed behaves as a vector.

4 Discussion

We have proven that the method of phase and group velocity tracing is accurate to measure the projection phase and group velocities of wave packet motion along any oblique direction. With the additional information of radial group velocity v_{gr}, it becomes possible to precisely obtain all the properties of the gravity wave if the projection mean wind u_h is available. Therefore, simultaneous measurement of neutral wind in the region of QP echoes is critical to fully uncover the relation between QP echoes and their responsible gravity waves.

The main features of the QP echoes detected by MU radar (Yamamoto et al., 1991) were: (1) they appeared intermittently in time with periods of 5 to 10 min, (2) their range rates were in the range −60∼−90 m/s, (3) the ratio between the slopes of the striations and the line across the striations were positive and large, in general, with one exception showing a negative value. These features were successfully reproduced by our theoretical calculations of the projection movement (along the radar beam) of the wave packets of the specific atmospheric gravity waves, with their wave fronts parallel to the magnetic field line (see Table 3). On the contrary, these features were not reproduced by the calculations when the wave fronts were not parallel to the magnetic field line (see Tables 1 and 2). We also notice that all the vertical group velocities of these waves are positive, meaning that they might originate from lower altitudes.

There is one question which remains to be cleared: does the FAI drift velocity represent the characteristic horizontal phase velocity v_{ph} or the horizontal group velocity v_{gh} of the gravity wave packet, responsible for the generation of QP echoes? As clearly demonstrated in Tables 1–3, v_{gh} and v_{ph} are significantly different because v_{gh} is strongly modulated by the projection mean wind u_h, so it is necessary to distinguish one from the other. Unfortunately, it is impossible to give a clear answer unless the projection mean wind is simultaneously available. Nevertheless, by theoretical calculations to obtain Table 3, we were able to obtain some gravity wave packets qualitatively matching QP echoes regarding FAI drift velocity as horizontal phase velocity. On the contrary, our efforts had failed to obtain meaningful wave packets matching QP echoes when we regarded it as the horizontal group velocity.

Appendix A

Method of phase- and group-velocity tracing

An RTI plot of the local power of $\Psi(r,t)$ (generated by Eq. (13) in the text) can be obtained by the following procedure (Kuo et al., 1998): At each time step $t_i{=}i\,\Delta t$ and radial range $r_k{=}k\Delta r$, a time series of N data points (N is chosen to be 15 in this paper) is defined by

$$\left\{\Psi_{\ell k}=\Psi\left(r_k,t_\ell\right),\ell=i-\tfrac{N}{2},i-\tfrac{N}{2}+1,...,i+\tfrac{N}{2}\right\}. \quad \text{(A1)}$$

First, to remove the very long period wave contribution, a linear trend of this time series (Eq. A1), $y{=}at{+}b$, is obtained by the method of least-squares-fitting, then a new time series (Eq. A2) is obtained from Eq. (A1) by subtracting its linear trend:

$$\left\{\Psi'_{\ell k}=\Psi_{\ell k}-at_\ell-b,\ell{=}i{-}\tfrac{N}{2},i{-}\tfrac{N}{2}+1,...,i+\tfrac{N}{2}\right\}. \quad \text{(A2)}$$

Then, the time series (Eq. A2) is Fourier analyzed to obtain the power P_{ki} of the first harmonic. Considering P_{ki} as an index of the strength of the wave activity at radial range r_k and time t_i, we plot the matrix $[P_{ki}]$ as an RTI plot for investigation (we use the contour plot to represent the RTI plot in this paper). A numerical simulation study (Kuo et al., 1998) showed that when a wave packet is propagating, packets with high regularity would exist in the RTI plot. It was shown that the same phase points of the characteristic wave component of the wave packet form a straight line called a phase trajectory, while the centers of the neighboring packets form another straight line called an energy trajectory. It was also noticed that the former determines the direction of the phase progression and the latter constitutes the direction of energy propagation. Therefore the slope of the phase trajectory is just the phase velocity and the slope of the energy trajectory is the group velocity of the wave packet. Also, the horizontal distance between the two consecutive packets (corresponding to the peaks and the dips in the oscillation profile) equals one-half of the period of the characteristic wave component of the packet.

Acknowledgements. The authors are indebted to the referee for his/her patience in reviewing this manuscript, and bringing the nonlocal effect on the gradient drift instability to our attention. This work is supported in part by the National Science Council of Taiwan under the contract number NSC 94-2111-M-238-001 and NSC 95-2111-M-224-001.

Topical Editor M. Pinnock thanks S. Saito for his help in evaluating this paper.

References

Bernhardt, P. A., Selcher, C. A., Siefring, C., Wilkens, M., Compton, C., Bust, G., Yamamoto, M., Fukao, S., Ono, T., Wakabayashi, M., and Mori, H.: Radio tomographic imaging of sporadic E-layers during SEEK-2, Ann. Geophys., 23, 2357–2368, 2005, http://www.ann-geophys.net/23/2357/2005/.

Cosgrove, R. B. and Tsunoda, R. T.: A direction- dependent instability of sporadic E-layers in the nighttime mid-latitude ionosphere, Geophys. Res. Lett., 29(18), 1864, doi:10.1029/2002GL014669, 2002.

Cosgrove, R. B. and Tsunoda, R. T.: Simulation of the nonlinear evolution of the sporadic E-layer instability in the nighttime mid-latitude ionosphere, J. Geophys. Res., 108(A7), 1283, doi:10.1029/2002JA009728, 2003.

Fejer, B. G., Farley, D. T., Balsley, B. B., and Woodman, R. F.: Vertical structure of the VHF backscattering region in the equatorial electrojet and the gradient drift instability, J. Geophys. Res., 80, 1313–1324, 1975.

Fukao, S., Yamamoto, M., Tsunoda, R. T., Hayakawa, H., and Mukai, T.: The SEEK (Sporadic- E Experiment over Kyushu) Campaign, Geophys. Res. Lett., 25, 1761–1764, 1998.

Hysell, D. L., Larsen, M. F., and Zhou, Q. H.: Common volume coherent and incoherent scatter radar observations of mid-latitude sporadic E-layers and QP echoes, Ann. Geophys., 22(9), 3277–3290, 2004.

Kuo, F. S., Lue, H. Y., and Luo, C. L.: Physical parameters of gravity wave packet propagation contained in radar RTI plots, J. Atmos. Solar Terr. Phys., 60(4), 455–460, 1998.

Kuo, F. S., Röttger, J., and Lue, H. Y.: Propagation of gravity wave packets in the lower atmosphere observed by the SOUSY-Svalbard radar, Chinese J. Phys., 41(4), 309–325, 2003.

Kuo, F. S. and Röttger, J.: Horizontal wavelength of gravity wave in the lower atmosphere measured by the SOUSY Svalbard Radar, Chinese J. Phys., 43(3–1), 464–480, 2005.

Larsen, M. F., Fukao, S., Yamamoto, M., Tsunoda, R. T., Igarashi, K., and Ono, T.: The SEEK chemical release experiment: Observed neutral wind profile in a region of sporadic E, Geophys. Res. Lett., 25(11), 1789–1792, 1998.

Larsen, M. F.: A shear instability seeding mechanism for quasi-periodic radar echoes, J. Geophys. Res., 105, 24 931–24 940, 2000.

Larsen, M. F., Yamamoto, M., Fukao, S., Saito, A., and Tsunoda, R. T.: SEEK-2: Observations of neutral winds, wind shears, and wave structure during a sporadic E/QP- event, Ann. Geophys.,

23, 2369–2375, 2005,
http://www.ann-geophys.net/23/2369/2005/.

Maruyama, T., Fukao, S., and Yamamoto, M.: A possible mechanism for echo-striation generation of radar backscatter from mid-latitude sporadic E, Radio Sci., 35, 1155–1164, 2000.

Maruyama, T., Saito, S., Yamamoto, M., and Fukao, S.: Simultaneous observation of sporadic E with a rapid-run ionosonde and VI backscatter radar, Ann. Geophys., 24, 153–162, 2006,
http://www.ann-geophys.net/24/153/2006/.

Nakamura, T., Tsuda, T., Miyakawa, H., Matsushita, Y., Fukunishi, H., Takahashi, Y., and Yamada, Y. : Propagation directions of gravity wave patterns observed in OH CCD images during the SEEK campaign, Geophys. Res. Lett., 25(11), 1793–1796, 1998.

Ogawa, T., Otsuka, Y., Onoma, F., Shiokawa, K., and Yamamoto, M.: The first coordinated observations of mid-latitude E-region quasi-periodic radar echoes and lower thermospheric 557.7-nm airglow, Ann. Geophys., 23, 2391–2399, 2005,
http://www.ann-geophys.net/23/2391/2005/.

Ogawa, T., Yamamoto, M., and Fukao, S.: MU radar observations of turbulence and movement of the mid-latitude sporadic E irregularities, J. Geophys. Res., 100, 12 173–12 188, 1995.

Ogawa, T., Takahashi, O., Otsuka, Y., Nozaki, K., Yamamoto, M., and Kita, K.: Simultaneous middle and upper atmosphere radar and ionospheric sounder observations of mid-latitude E-region irregularities and sporadic E-layer, J. Geophys. Res., 107(A10), 1275, doi:10.1029/2001JA900176, 2002.

Onoma, F., Otsuka, Y., Shiokawa, K., Ogawa, T., Yamamoto, M., Fukao, S., and Saito, S.: Relationship between gravity waves in OH and OI airglow images and VHF radar backscatter from E-region field-aligned irregularities during SEEK-2 campaign, Ann. Geophys., 23, 2385–2390, 2005,
http://www.ann-geophys.net/23/2385/2005/.

Pfaff, R. F., Freudenreich, H., Yokoyama, T., Yamamoto, M., Fukao, S., and Mori, H.: Electric field measurements of DC and long wavelength structures associated with sporadic E-layers and QP radar echoes, Ann. Geophys., 23, 2310–2334, 2005,
http://www.ann-geophys.net/23/2310/2005/.

Riggin, D., Swartz, W. E., Providakes, J., and Farley, D. T.: Radar studies of long-wavelength waves associated with mid-latitude sporadic E layers, J. Geophys. Res., 91, 8011–8024, 1986.

Saito, S., Yamamoto, M., Fukao, S., Marumoto, M., and Tsunoda, R. T.: Radar observations of field-aligned plasma irregularities in the SEEK-2 campaign, Ann. Geophys., 23, 2307–2318, 2005, http://www.ann-geophys.net/23/2307/2005/.

Tanaka, T. and Venkateswaran, S. V.: Characteristics of field-aligned E-region irregularities over Iioka (36° N) Japan-I, J. Atmos. Terr. Phys., 44, 381–393, 1982.

Tsunoda, R. T., Fukao, S., and Yamamoto, M.: On the origin of quasi-periodic radar backscatter from mid-latitude sporadic E, Radio Sci., 29, 349–365, 1994.

Wakabayashi, M. and Ono, T.: Multi-layers structure of mid-latitude sporadic E observed during the SEEK-2 campaign, Ann. Geophys., 23, 2347–2355, 2005,
http://www.ann-geophys.net/23/2347/2005/.

Woodman, R. F., Yamamoto, M., and Fukao, S.: Gravity wave modulations of gradient drift instabilities in mid-latitude sporadic E irregularities, Geopgys. Res. Lett., 18, 1197–1200, 1991.

Yamamoto, M., Fukao, S., Woodman, R. F., Ogawa, T., Tsuda, T., and Kato, S.: Mid-latitude E region field-aligned irregularities observed with the MU radar, J. Geophys. Res., 96, 15 943–15 949, 1991.

Yamamoto, M., Komoda, N., Fukao, S., Tsunoda, R. T., Ogawa, T., and Tsuda, T.: Spatial structure of the E-region field-aligned irregularities revealed by the MU radar, Radio Sci., 29, 337–347, 1994.

Yamamoto, M., Fukao, S., Tsunoda, R. T., Pfaff, R., and Hayakawa, H.: SEEK-2 (Sporadic- E Experiment over Kyushu 2) – Projet Outline, and Significance, Ann. Geophys., 23, 2295–2305, 2005, http://www.ann-geophys.net/23/2295/2005/.

Yokoyama, T., Yamamoto, M., and Fukao, S.: Computer simulation of polarization electric fields as a source of mid-latitude field-aligned irregularities, J. Geophys. Res., 108(A2), 1054, doi:10.1029/2002JA009513.2003.

Yokoyama, T., Yamamoto, M., Fukao, S., and Cosgrove, R. B.: Three-dimensional simulation on generation of polarization electric field in the mid-latitude E-region ionosphere, J. Geophys. Res., 109, A01309, doi:10.1029/2003JA010238, 2004.

Yokoyama, T., Yamamoto, M., Fukao, S., Takahashi, T., and Tanaka, M.: Numerical simulation of mid-latitude ionospheric E-region based on SEEK and SEEK-2 observations, Ann. Geophys., 23, 2377–2384, 2005,
http://www.ann-geophys.net/23/2377/2005/.